

Framework for Computer-aided Detection of Pulmonary Embolism

Raphaël Sebbe, Bernard Gosselin, Roger Lédée, Christophe Léger,
Emmanuel Coche & Benoît Macq^{*†‡§}

^{*}R. Sebbe, Ir. and Prof. B. Gosselin, are with the TCTS Lab, Faculté Polytechnique de Mons, 1, avenue Copernic 7000 Mons, Belgium (email: raphael.sebbe@tcts.fpms.ac.be)

[†]R. Lédée, PhD., and C. Léger, PhD., are with the LESI Lab, University of Orléans, 12 rue de Blois BP 6744, 45067 Orléans, France (email: Roger.Ledee@univ-orleans.fr)

[‡]E. Coche, MD., PhD., is with the Department of Medical Imaging, Université catholique de Louvain, Cliniques universitaires, St-Luc, 10, avenue d'Hippocrate, 1200 Brussels, Belgium (email: coche@rdgn.ucl.ac.be)

[§]Prof. B. Macq is with the Telecommunication Lab, 2, Place du Levant, 1348 Louvain-la-Neuve Belgium (email: macq@tele.ucl.ac.be)

Submitted: 15th October 2018

Revised: 30th December 2018

Accepted: 13th March 2019

In this paper, we present a framework for computer-aided diagnosis of pulmonary embolism (PE) in contrast-enhanced computed tomography (CT) images. It consists of a combination of a method for segmenting the pulmonary arteries (PA), emboli detection methods as well as a scheme for the evaluation of the performance. The segmentation of the PA serves one of the clot detection methods, and is carried out through a region growing method that makes use of a priori knowledge of vessels topology. Two different approaches for clot detection are introduced: the first one performs clot detection by analysing the concavities in the segmentation of the pulmonary arterial tree. It works in a semi-automatic way and enables the detection of thrombi in the larger sections of the PA. The second method does not make use of the segmentation and is thus fully automatic, enabling detection of the clots farther in the vessels. The combination of these methods provides a robust detection of clots that can be used as a safeguard by radiologists, or even as preliminary computer-aided detection (CAD) toolset. The evaluation of the method is also discussed, and a scheme for measuring its performance in terms of sensitivity and specificity is proposed, including a practical approach to making reference detection data, or ground truths, by radiologists. Results are presented and discussed.

1. INTRODUCTION

Pulmonary embolism (PE) is an extremely common and highly lethal condition that is a leading cause of death in all age groups. Its symptoms are often vague and its diagnosis is a major medical challenge. However, when properly identified, an efficient treatment exists that dramatically reduces the mortality rate of the disease. Multislice computed tomography (CT) has gained acceptance as a minimally invasive method for evaluating patients with suspicion of PE [1]. Nowadays, the diagnosis of PE is manually performed by radiologists on CT scans, and it is a time-consuming and error-prone process, in particular because of the huge amount of data and more specifically in the case of sub-segmental and peripheral clots, which are more difficult to locate. In that context, a computer aid can be provided to act at least as a safeguard for radiologists or even better, if sufficiently conservative, as a preliminary detection means.

In this paper, we propose a framework for the problem of detection of PE in contrast-enhanced CT images. This framework permits the use of various clot detection methods that are eventually combined to provide final detection results. For the sake of completeness, we note at this point that a classification method could be implemented as well,

whose role would be to decrease the false alarm rate, but this was not investigated in this study. Two clot detection methods are presented. The first one uses a segmentation of the PA as a semi-automatic process, while the second one works directly on image data and is a fully automatic process. The segmentation of the PA is a challenging task by itself, and, considering our specific application where images are contrast-enhanced (Fig. 1), meaning that a contrast product is used to opacify¹ the arteries, we developed a model-based active contour method. The algorithm used for region growing is based on the fast marching algorithm first developed by Sethian *et al.* [2]. Later on, our early segmentation results showed that touching vessels, that is, neighboring thorax vessels with no visible frontier between them in the image, were an important issue for region growing-based methods. We used an a priori model to handle the case these joint vessels, that would otherwise lead to the segmentation of other thorax vessels. This model is made of a set of parametric 3D curves that represent the centerlines of the vessels, and is used in the active contour step by modifying the expression of the speed of propagation.

The first clot detection method looks for holes or concavities in the segmentation of the PA that correspond to clots. It does so by applying a set of operators of

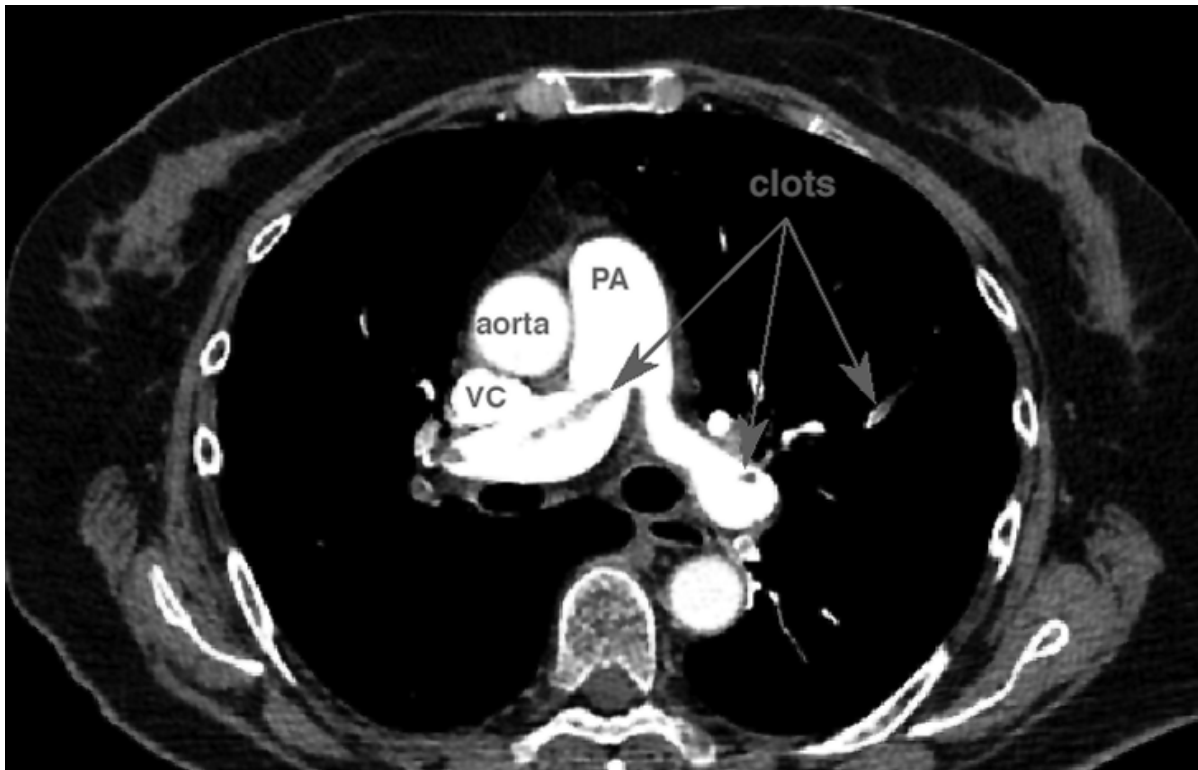


Figure 1: Illustration of a typical slice of a CT volume, with opacified vessels. Main thorax vessels are identified, and emboli are marked by an arrow.

thresholding, 3D mathematical morphology [3] and logical operations. The second detection method makes assumptions about the density and the shape of the clots to identify them. Because simple criteria are used, this method leads to many false positives, and a lot of which are outside of the lung volume. Lung volume segmentation is used to tackle that situation. Both clots detection methods are combined and provide a 3D, voxel-wise mask of emboli presence.

Eventually, a scheme for assessing the performance of a PE detection method is introduced. It focuses on the creation of ground truth data by radiologists that permits a comparison with the results of the detection methods, in terms of false negative (non-detections) and false positive (false detection) rates, which lead to method sensitivity and specificity. That scheme is used with our method and the results are discussed.

This paper is organized as follows: related work is covered in the next section. After that, the algorithm for segmenting the pulmonary arteries is presented, as well as both emboli detection methods. Eventually, evaluation and results are discussed and a conclusion is drawn.

2. RELATED WORK AND MOTIVATIONS

Vessels analysis in both 2D and 3D image datasets has attracted many research efforts in the recent years. One approach to the problem of emboli detection is to first extract the pulmonary arteries. Depending on modality and the kind of studied vessels, whose sizes and shapes may vary, different vessels segmentation methods have been used. Kirbas *et al.* did a classification of vessels extraction methods in [4], and

Felkel [5] did a review that is more specific to the case of contrast enhanced images (CTA - computed tomography angiography). What comes out is that region growing method provide a superior ability to segment this type of variable scale structure. The first application of region growing methods to vessels in 3D dataset is attributed to Zahlten *et al.* [6]. Their method handles the bifurcation of vessels and simultaneously reconstructs the hierarchical structure of the vessels tree. More recently, active contours methods have been used for segmenting vessels. Snakes permit the segmentation of organs in 2D (3D extensions also exist) but *level sets* and *fast marching* algorithms introduced by Sethian and Malladi are better suited to elongated structures than snakes [2, 7], because of their easy extension to 3D and their topology adaptation capability. Deschamps *et al.* presented a method based on the *fast marching* algorithm for 3D vessels segmentation [8, 9], adding the concept of freezing contour evolution once the vessel boundaries are reached. Using a similar concept, we presented our *slice marching* method in [10], and later extended it with the use of a model in [11] to handle the case of touching vessels.

Back to the detection problem, Masutani *et al.* presented a method for emboli detection based on the segmentation of the PA [12], whose main limitation is that its results are tightly linked to the quality of the underlying PA segmentation. Another approach to emboli detection is not to use any prior segmentation of the PA. Such an approach, based on tobogganing, was recently presented in [13]. That method gives very good sensitivity and its main drawback

seems to be the high number of false positives. This is not much discussed, and the way to compute that false alarm rate is not expressed. As we found out, segmentation of lung volume can dramatically reduce false positives rate for that kind of methods. Segmentation of the lung volume was studied by van Ginneken *et al.* for radiographs [14], and we note that the problem is easier in CT scans, because of the access to unprojected raw data. Interest in emboli detection based on machine learning methods and classification was recently expressed [15], but this was not studied as part of this work, although it might be a way to further refine the detection results. Eventually, we also note that up to this time, little efforts have been made to provide a standard means for assessing PE detection methods.

Our research efforts first focused on the development of a PA segmentation method that handles the case of touching vessels, and later on the PE detection problem. Our solution to the segmentation problem begins with an approach similar to Deschamps *et al.* [8], adding support for touching vessels by using a model of thorax vessels. For the detection problem, we combine a method based on PA segmentation with another one that is not, in the hope of coping with their individual weaknesses. Eventually, we propose a standard scheme for assessing automatic PE detection algorithms and discuss the results when that scheme is applied to our detection method.

3. METHODS

3.1 Preprocessing

By studying how radiologists perform the analysis of the image-volume in the context of emboli detection, we noticed that not all 12-bit gamut of voxels are generally used. Instead Hounsfield Units (HU) in the range of [0,350] (out of [-1000, +3000]) suffice. HUs are typically mapped in the 8-bit scale of console displays, that range containing most of the interesting information regarding this application. This first processing step performs exactly that.

3.2 Segmentation of the PA

3.2.1 Front Propagation

Starting from a seed point at the beginning of the PA, we let a 3D contour, or surface, grow. To accomplish this, we want to solve the Eikonal equation (1) using the *fast marching* algorithm, as expressed by Sethian [2]. Given an initial contour where the crossing time, T , is known to be zero, (curve in 2D, surface in 3D) and given its speed of propagation along its normal at every point in the image, $F(\bar{X})$, we compute the solution $T(\bar{X})$ to the Eikonal equation (1) at every voxel \bar{X} :

$$|\nabla T(\bar{X})| F(\bar{X}) = 1, \text{ with } T(\bar{X}) = 0 \text{ on the seed} \quad (1)$$

If we suspend the computation of the solution when the crossing time $T(\bar{X})$ becomes higher than a given threshold T_{slice} ,

$$\text{if } (T(\bar{X}) > T_{slice}) \Rightarrow \text{suspend} \quad (2)$$

and if we define our speed function $F(\bar{X})$ so that it is near to one inside the vessel, and by noticing that time and distance are equivalent when speed is unity, we can tell that T_{slice} is the depth of the slice. An estimate of the section of the vessel can be made by dividing the slice volume by its depth.

Next, by choosing a speed function $F(\bar{X})$ that is small enough outside the vessel, we can freeze the active front (denoted as the *trial* set in the *fast marching* algorithm [2]) by not considering voxels whose arrival time is higher than a second threshold, T_{bound} :

$$\text{if } (T(\bar{X}_i) > T_{bound}) \Rightarrow \text{remove } \bar{X}_i \text{ from trial set} \quad (3)$$

Then, we iterate using a time threshold T_{slice} of the form:

$$T_{slice} = T_k = k \Delta T_{slice} \quad (4)$$

ΔT_{slice} being the depth of the slice, each time getting a new slice. We define a slice \mathcal{S}_k as:

$$\mathcal{S}_k, \triangleq \{ \bar{X} \mid T_k \leq T(\bar{X}) < T_{k+1} \} \quad (5)$$

where a temporal criterion actually defines spatial zones².

The speed function should be near one inside the vessel, and near zero outside. Moreover, in the *fast marching* method, the propagation speed is required to be strictly positive. Considering an input voxel density $I(\bar{X})$ between 0 and 1, we provide the corresponding speed by

$$\begin{aligned} F &= \epsilon && \text{if } I(\bar{X}) < I_{th} \\ &= I(\bar{X}) && \text{otherwise} \end{aligned} \quad (6)$$

where ϵ is a positive, near zero value and I_{th} a threshold on luminance (we used a value of 90%, using the hypothesis that vessels are correctly opacified). A hard threshold (0 or 1) was not used to enable the method to tackle the case of opacification noise (small and local decrease), where vessels are not generally totally white.

3.2.2 Detection of Bifurcations

As the front advances inside the vessels for recovering the entire arterial tree, a hierarchical structure of the vessels is built. Voxels of slices of the same generation (same k) are checked for their mutual connectivity (connected component analysis). Unconnected groups of voxels define as many slices.

3.2.3 Adding Anatomical Knowledge Model

Considering the presence of contacts between vessels, or touching vessels, in terms of image intensity (they are not linked anatomically), we understand that methods only based on the voxel-wise information in the image cannot handle it. Segmentation fails by oversegmenting when limited resolution, noise, and artifacts tend to merge adjacent but physically separate vessels. What we observe in that case is

that the active contour moves from the PA to the nearby vessels, e.g. the vena cava and then the aorta.

It seems difficult to handle that problem with no prior information, as the “touching” area can actually be bigger than the section of one of the vessels involved. A medical solution is not practical to solve this problem. Indeed, varying the timing and the rate of the injection of contrast medium to opacify the PA alone is not practically reproducible. Moreover, we have found this situation to be recurring. This leads to the development of a specific solution. To achieve this, we use an a priori anatomical knowledge, as practitioners do.

Basically, we want to represent the topology and shape of vessels using a mathematical, parametric model. Next, that model can be used to influence the way the active front propagates inside the vessel, and, in particular, to recreate missing vessel boundaries. We also want to share that model across patients (as creating it can be a tedious process), and for this reason, it has to be registered with the CT image of the patient.

Each thorax vessel is modeled as their centerline and mean radius. The centerline is defined as a parametric, 3D, fourth order Bézier curve. Another class of curves, such as B-Spline, NURBs, etc. could have been used but Bézier splines have the advantage of passing through their control points, which is what we are looking for (radiologist clicks where the curve should go)³.

A vessel section (part between two bifurcations) is modeled as a number of Bézier segments. A Bézier segment of order 4 is defined as a set of 4 control points with the property that the curve interpolates the first and the last control points. Continuity is maintained between segments by constraints on the control points of nearby segments. A hierarchical tree of vessel sections is built when creating the model.

Such a model is represented in Fig. 3. There, we can see that the aorta has an associated model, so has the PA, including bifurcations.

We define a vessel potential function, $P(\bar{X})$, as

$$P_i(\bar{X}) = R_i / D_i(\bar{X}) \quad (8)$$

i refers to the vessel section⁴ being considered, R_i is the mean radius for the vessel section, $D_i(\bar{X})$ is the Euclidian distance between \bar{X} and the nearest point on the centerline of vessel i . R_i is manually estimated on a chosen patient with visual tools for each vessel section, the important information being the relative sizes of the vessels.

From the potential function, we derive the vessel interior indicator, $V(\bar{X})$ as

$$V(\bar{X}) = 1 \quad \text{if} \quad \max_i (P_i(\bar{X})) - \max_{j \neq i_{\max}} (P_j(\bar{X})) > \lambda \quad (9)$$

$$\epsilon \quad \text{otherwise} \quad (10)$$

with $i_{\max} = \arg(\max_i (P_i(\bar{X})))$. λ is a parameter ($\lambda > 0$) that

can be used to adjust the reconstructed boundaries width, and ϵ a positive value near zero.

The vessel potential is used to modify the speed of propagation of the active front:

$$F'(\bar{X}) = F(\bar{X}) \times V(\bar{X}) \quad (11)$$

We built the function $V(\bar{X})$ in order that it is near zero when neighboring vessels potentials are the same (potential collision). This has the effect of recreating the possibly missing vessel boundaries ($V(\bar{X})$ imposes the boundary). On the contrary, when the vessel is alone (not surrounded by other vessels too closely), then, the image imposes the boundary (as it did before using model). This is illustrated on Fig. 2. ($V(\bar{X})$ is computed on a sub-sampled 3D grid (by a factor 8) using a distance map algorithm as the ones proposed by Cuisenaire [16], and piecewise linearly interpolated for in-between voxels.

As expressed before, we intend to provide a single model that can be reused across patients. To achieve this

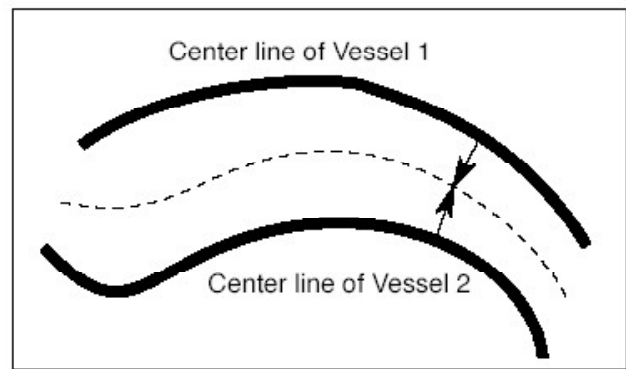


Figure 2: The model is used to create missing vessel boundaries. The dotted line shows the boundary that is created from the vessel center lines (that boundary is a surface in 3D).

goal, we decided to set a limited number of fiducial points in the model space that can be easily located in the image of a new patient. Once the association has been made between the two, the model is then deformed using the thin-plate algorithm [17], which provides a non-linear, continuous space transformation that applies a set of points to another. This is illustrated in Fig. 3.

Practically, the parametric model is created on the image volume of a chosen patient, where principal vessels centerline are modeled as 3D Bézier curves. The set of fiducial points is also defined on that image, each point being given a detailed description of its location in anatomical terms so that it can be found on any patient. That set of points should be spread around the model in a way that the induced transformation correctly applies it to another patient. Based on the hypothesis that the circulatory system in the thorax is very similar across patients (at least to a certain number of bifurcations), we used a limited number of 7 fiducial points that provide sufficient accuracy in

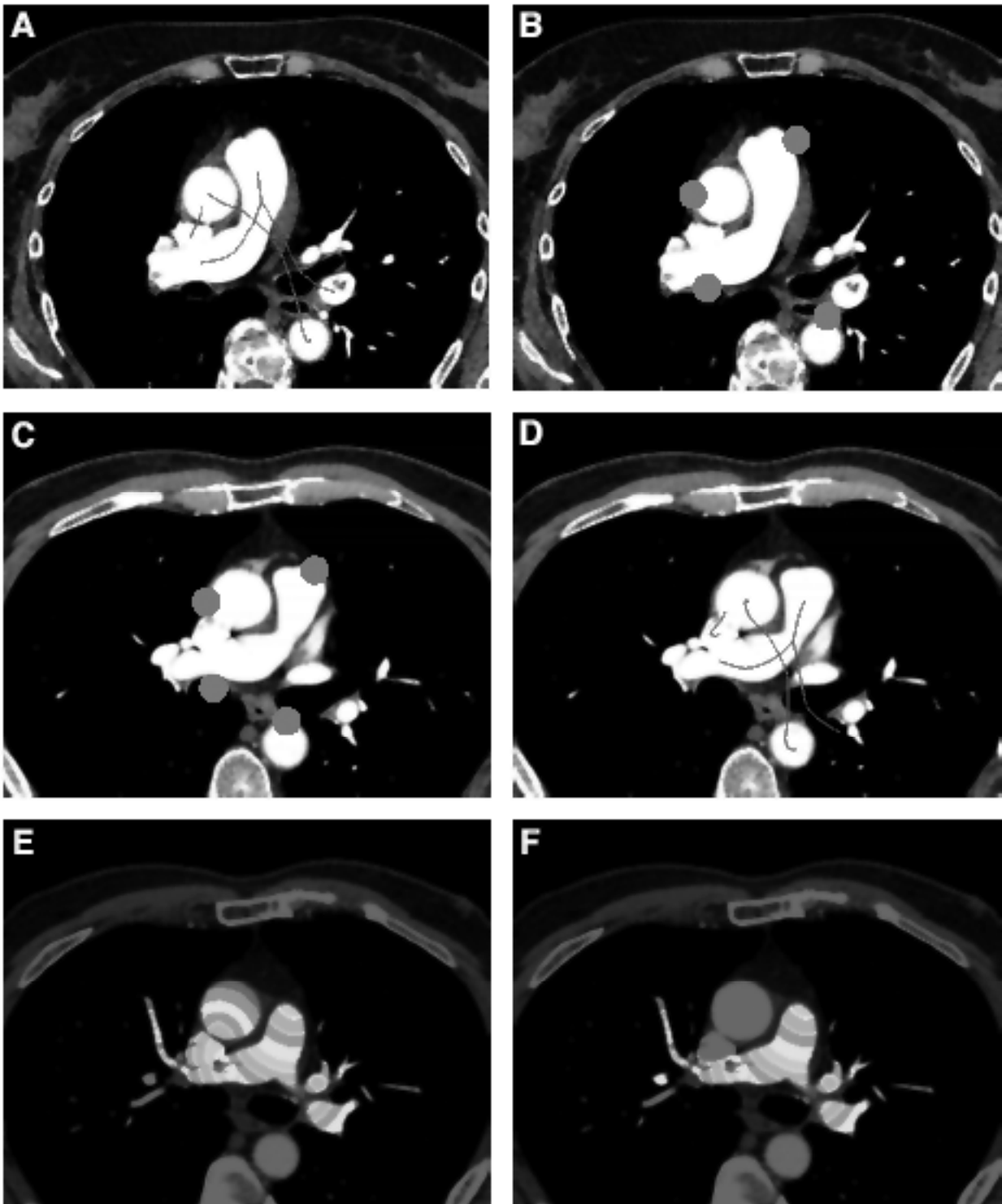


Figure 3: Model influence on PA segmentation. (A) shows a model corresponding to a particular image, and (B) a chosen set of fiducial points for that image. The fiducial points are localized on another patient image, (C), and that correspondence is used to adapt the model to the new patient (D). (E) and (F) respectively shows segmentation without using the model, and with. In (E), the vena cava and aorta are incorrectly segmented, and correctly avoided in (F).

modeling the scale adaptation and simple non linear transformation, with limited expense in localization time. Although the reconstructed boundary may be different from the actual one, this weak co-registration nonetheless permits to stop the front from moving to adjacent vessels.

When a new image is obtained, the first step is to locate the chosen set of fiducial points on it. Making the correspondence with the reference set of points enables us to evaluate the thin plate transform that applies the model to the new image.

3.2.4 Switching off the Model

The model can be used where vessels topology or shapes is not dependent on the patient. This is verified for most thorax vessels, as the aorta, vena cava and the main trunk of the pulmonary arteries and veins. These last two vessels present a higher variability in shapes as ones goes farther from the heart. For this reason, we have to stop modeling these past a given number of bifurcations. Switching off model usage is accomplished, and rules are added to keep control of contour evolution past this point. In particular, we want to prevent the contour from going back to the heart through the veins from a contact point with a segmented artery. This is made by measuring the mean section of the vessels while segmenting them and by banning a section increase.

3.3 Emboli Detection based on PA Segmentation

This method is referred to as *M1* later on. The idea behind this method is to find darker concavities, going from the segmentation mask of the PA. This is accomplished by using a set of morphological and thresholding operators. The block diagram is depicted on Fig. 4

3.3.1 Processing

By nature, this segmentation technique leaves the clots out of the resulting segmentation mask, because of their lower contrast. Depending on the clot position in the vessel, 2 cases show up:

- there is a contact between the clot and the boundary of the vessel,
- or there is no contact.

In the former case, the segmentation mask will generally present a concavity. In the latter case, a hole is present in the mask. This only makes sense when considering the

neighborhood of a chosen region in the vessel, because in general, an embolus may have a very elongated shape, comparable to a vessel inside a vessel whose boundary may touch locally. What has to be considered as well is that not all concavities in the segmentation mask do represent a clot, although this method will classify them as such (false alarms).

The first step in this approach is to decrease acquisition noise, yet preserving edges. Basically, we want to get mostly homogeneous regions in terms of voxel intensity for the different relevant classes (white, grey, black), thus avoiding salt and pepper kinds of noises. This is done through bilateral filtering [18] for each 2D image in the volume. Median filtering could have been used as well.

The second step is to perform the closing, in the sense of mathematical morphology, of the segmentation mask to retrieve its concavities and holes. Although it makes sense to have a variable size for the structuring element (SE) [19], depending on the size of the nearby vessels, we did not experience it. The shape of the SE is a 3D box and its size is $12 \times 12 \times 12$ voxels (which corresponds to a 12mm cube). The chosen size must be bigger than the largest embolus we want to be able to detect. A 3-D rectangular shape was chosen for the SE for performance reasons, although a spherical one could provide less synthetic (axis aligned) detection shapes.

In the last step, we combine the difference between the original segmentation mask and the closed one, with the mask identifying the interesting grey regions using a voxel-wise and operator. The 2 thresholds (low, high) are easily chosen because a contrast product is used, but may depend on scanner brand.

The detection result of method *M1* can be superimposed to the original image, showing the voxel-wise detection. This is illustrated on Fig. 5.

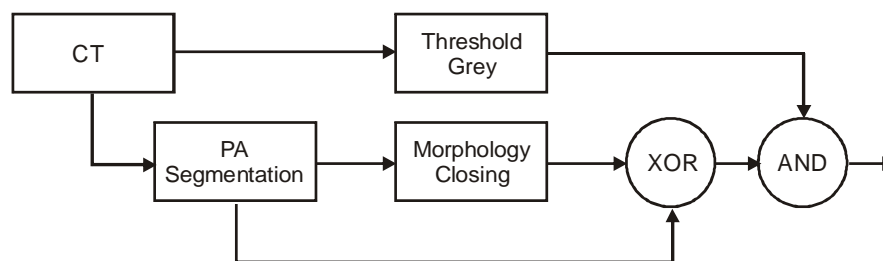


Figure 4: Method M1 diagram. PA segmentation is computed from the CT data, then fed into a morphology closing. The difference between the closing and the original segmentation gives the clots candidate mask, whose intersection with the grey mask is computed.



Figure 5: Detection result of method M1. Left: original image, center: PA segmentation mask, right: emboli detection mask.

3.3.2 Limitations

This method has several limitations. Firstly, as it is based on PA segmentation, it cannot detect clots where the segmentation fails. Segmentation can fail for various reasons, in particular if one artery is completely obstructed by a clot. Secondly, another problematic case is when going farther in the arteries tree (smaller vessels), clots may no longer show up as concavities in the segmentation mask. We overcome these in method *M2*.

3.4 Standalone Detection

This method is referred to as *M2* later in this paper. The idea behind this method is to go through the entire image volume and find clots based on shape and density properties. The segmentation of the lung volume is performed to limit the rate of false positives. Method diagram is on Fig. 6.

3.4.1 Emboli Detection

If we go back to the definition of a clot in image terms, we could model its shape and color as a *grey cylinder* in 3D space, at least locally. This definition remains correct even if the embolus completely obstructs the vessel. Of course, this means that there is an additional constraint in the medical protocol, that is that not only the arteries must opacified, but also the veins and the other vessels of the thorax, otherwise they will be interpreted as clots.

Such a cylinder has at least one intersection with one of the three reference planes (*XY*, *YZ*, or *ZX*) whose section is an ellipse having an axis ratio in $[1/\sqrt{3}, 1]$, the value of one corresponding to a circle. This lead us to search for grey shapes, in all the planes slicing the volume that are parallel

to the reference planes, that meet this shape criterion. In practice, the clots are not perfect ellipses and their section has an upper bound (the size of the biggest artery).

We implemented this by first segmenting interesting grey regions (as expressed in 3.3.1) and performing connected component analysis. For each obtained component, we measure its perimeter and area and accept it if both its area is smaller than the largest accepted clot section, and its compactness ($4\pi \cdot \text{area} / \text{perimeter}^2$) is big enough (for an ellipse, the compactness value is about 0.896). Three traversals of the image volume are made, one for each reference plane, and the results are *or'ed* to provide the detection mask. An additional step of 3-D mathematical morphology opening is performed to assert a minimal space coherence in the detection, as clots generally show a minimum depth.

This detection method obviously considers many shapes as emboli candidates, because the associated hypothesis is easily met. What we could observe is that many of the false positives were lying outside of the interior volume of the lung. For this reason, the segmentation of the lung volume was performed to further constrain the detection.

3.4.2 Lung Segmentation

Many techniques can be considered to perform the lung segmentation task. Looking at the images, we see that lung air voxels have low densities (black voxels), and a method based on thresholding and connected components analysis is able to handle that. The block diagram of the method that we used is presented on Fig. 7. It is applied successively to each 2D slice, to retrieve the entire lung volume segmentation (illustrated on Fig. 8).

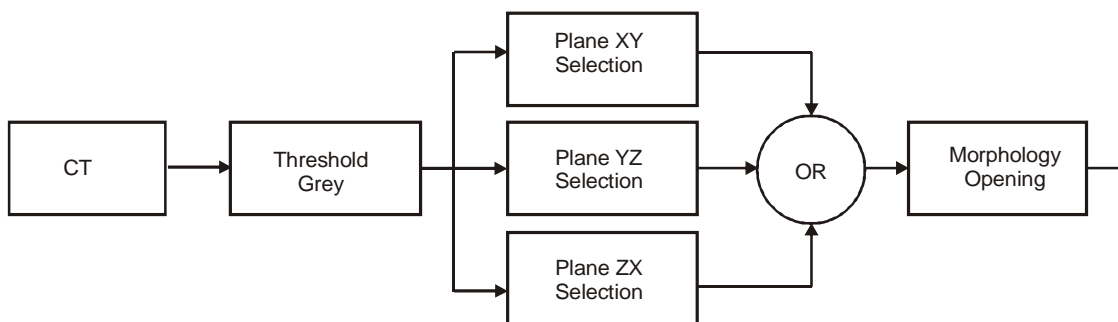


Figure 6: Method *M2* diagram. Grey thresholding is performed on the CT data. The volume is then swept through from the 3 reference planes, performing connected component analysis. The three results are added, and morphology opening is performed (clean erroneous isolated detections).

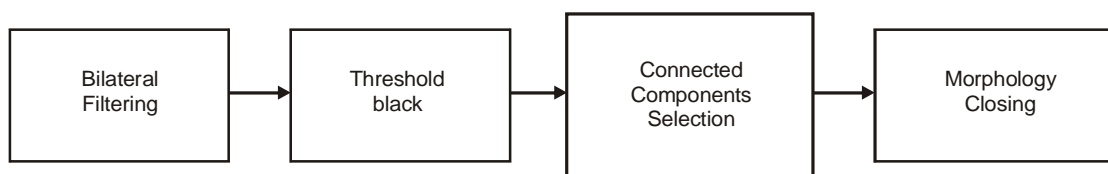


Figure 7: Lung segmentation. Bilateral filtering is used to smooth the image, black regions are segmented and searched for connected components. Connected components having a contact with image borders as well as the one not meeting a size criterion are discarded. Closing is then applied to retrieve thorax vessels and organs.

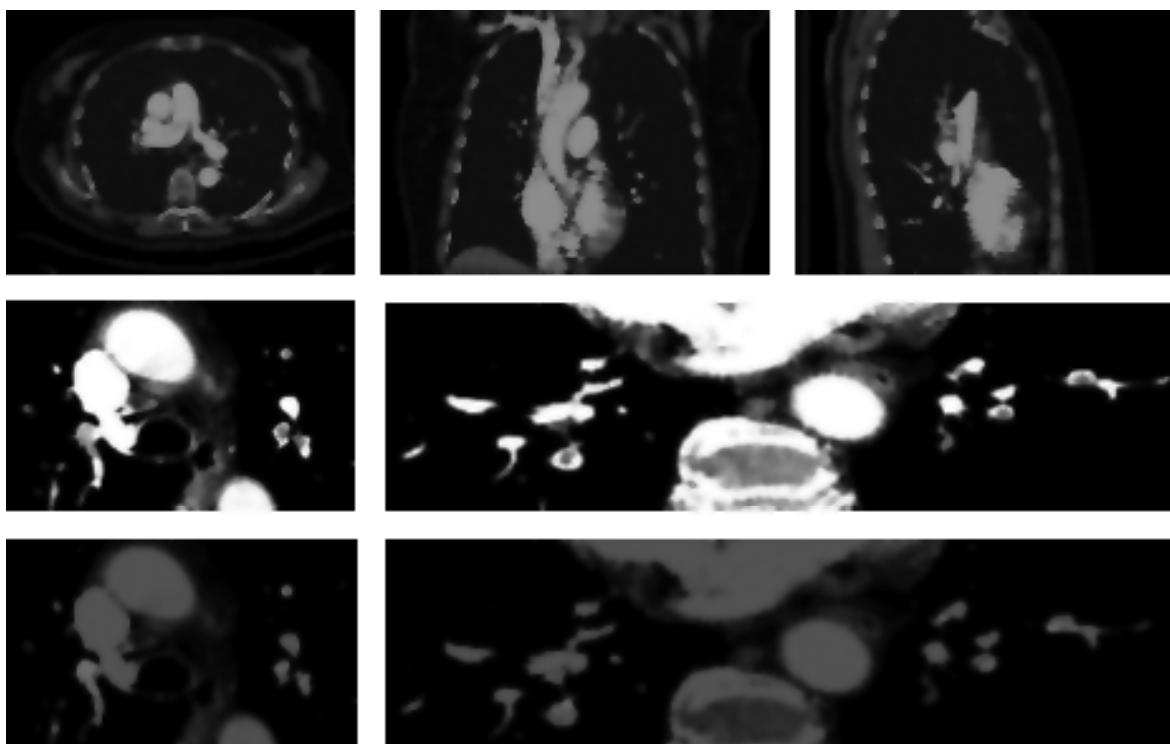


Figure 8: Results of method M2. The first row shows the lung segmentation (axial, coronal, sagittal slices), the second row the original image, and the last row the superimposed emboli detection mask.

3.5 Fusion

Both envisaged methods do not detect the same features. Combining both detection mask is made by a logical or operator to preserve all information, at the expense of keeping the false positives of the methods as well. A comparison of the detection results of both methods is depicted on Fig. 9.

4. VALIDATION

Assessing the quality of a detection method requires the intervention of experts, in this case, radiologists. Different

levels of assessment can be considered, that range from looking at the exam as a whole and reporting that a patient is affected by pulmonary embolism or not, to looking at every clot and report successful detection, to a voxel-wise classification (embolus or not). Our method by essence provides that latter information, but this may be different for other methods. Although it could be interesting to obtain ground truth data from radiologists as a voxel-wise classification, this is not practical due to the huge amount of work it would take. We came up with a scheme that would provide a compromise between accuracy and practical realization.



Figure 9: Both detection methods are compared. Method M1 correctly identifies a clot that partially obstructs the artery in the bottom part of this image, that M2 does not detect. To the contrary, the bigger clot above is only partially detected by M1, while M2 detects it accurately.

4.1 Ground Truth Definition

Previous work focused on reporting the success of detection for manually located thrombi [12] by considering them as a whole. Although this makes sense for clots of small sizes, in our datasets, part of the clots had an elongated shapes (up to about 10 centimeters). An evaluation scheme that reports how well the detection is performed for the entire clot is proposed.

In this scheme, proposed in [20], the ground truth is defined as a partition of voxel boxes of a chosen size, which are individually marked as containing a clot or not. The size of these boxes is an important parameter, lower sizes giving more precise information at the cost of a longer time needed to realize the ground truth. The chosen size also affects the results. We arbitrarily chose to use $16 \times 16 \times 16$ boxes. Practically, the radiologist navigates through the volume on which a 3D grid is painted, highlighting boxes that contain clots (either entirely or not). This is illustrated on Fig. 10.

The same information is constructed from the output of the detection method, and at the same resolution as the one chosen before. Both results (ground truth and detection algorithm) can then be compared.

Inter- and intra-radiologist variability has to be considered. Although it was not studied as part of this work, we can assume that this variability has different causes:

- Interpretation of image. Different radiologists interpret images differently.
- Border consideration. The delineation of clots along boxes borders can be ambiguous.

The first point is inherent to the detection process performed by experts. The second one is linked to the use of the tools, and addressing it can be done by providing a score or confidence instead of a boolean value stating the presence of clots. But this was not investigated at this time.

4.2 Measuring Sensitivity and Specificity

In traditional binary classification, false positives (FP) are defined as the cases where the detection method detect a clot while the expert does not. A *false negative* (FN) is the dual situation where experts detects a clot and the method does not. True positives (TP) and true negatives (TN) are for the cases when both agree, respectively detecting a clot (positive) and not detecting a clot (negative). Sensitivity (Sn) and specificity (Sp) are defined by the following formulas:

$$Sn = \frac{N_{TP}}{N_{TP} + N_{FN}}, \quad Sp = \frac{N_{TN}}{N_{TN} + N_{FP}}$$

where N_{TP} , N_{TN} , N_{FP} , and N_{FN} respectively are the number of occurrences of true positive, true negative, false positive, and false negative.

We note that both concepts do not have the same importance depending on the context in which they are used. In the medical diagnosis context, non-detections should generally be avoided as much as possible, as this can directly impact health-related consequences and a bad specificity

may impact the value of a computer-aided detection, or CAD, toolset.

5. RESULTS / DISCUSSION

We have tested this emboli detection method on 18 datasets obtained from multi-slice computed tomography, or MSCT, in patients addressed for suspicion of pulmonary embolism (PE) (clot within a pulmonary artery). CT examinations were performed using the following parameters: 16 X 0.75 mm slice thickness, 0.6 mm interval of reconstruction, 120 Kv, 150 mAs, pitch of 0.95, matrix size: 512 x 512, 12 bits per voxel. 100 mL of non ionic contrast medium was injected through an antecubital vein at a rate of 4 mL/sec with variable delay in order to opacify the PA. Different scanner machines were used at both sites (Siemens at CHR in Orléans, Philips at St-Luc Hospital in Brussels).

Ground truths were built for these images by a radiologist, where individual voxel boxes of $16 \times 16 \times 16$ are marked for the presence of emboli for the entire volume. All 18 patients were affected by pulmonary embolism, albeit to different degrees. The detection method was then confronted to the reference, Fig. 11 compares ground truths and the method for images of different patients. The comparison results are expressed visually, where true positives are shown in green, false positives in blue, and false negatives in red for each voxel box in the volume (volume slices are displayed).

5.1 Performance

In terms of sensitivity and specificity, the method performs as follows: sensitivity of 88.4% is achieved, as well as a specificity of 98.9%, with respective standard deviation of 10.4% and 0.39%. The sensitivity is high, and while it can still be increased, it already makes the method well suited for its original goal. The specificity is a little misleading, as it suggests that there are not many false alarms. This is due to the fact that the number of true negative boxes is big (working in 3D). Another way of considering the results is to look at how much data the radiologist would have to look at if he only considered the boxes marked as positive by the method. This is the ratio between positive-detected boxes to the total number of boxes, and in our datasets, its value was in [0.85%, 2.34%]. The higher the number of false alarms, the more often the radiologist will have to manually discard erroneous detections.

When looking more closely at each detection result taken individually, the worst sensitivity (57.9%) shows up for a case of massive embolism, where the most part of the PA is obstructed. In that case, hypothesis made by $M1$ and $M2$ are not met for the bigger clots. In one of the cases, the segmentation of the PA failed (the heart and other vessels were segmented as well, due to massively missing vessel boundaries), and false alarms for $M1$ consequently increased, yet overall sensitivity was not affected.

We can see that $M1$ detects properly the obvious clots within the main section of the PA, without many false

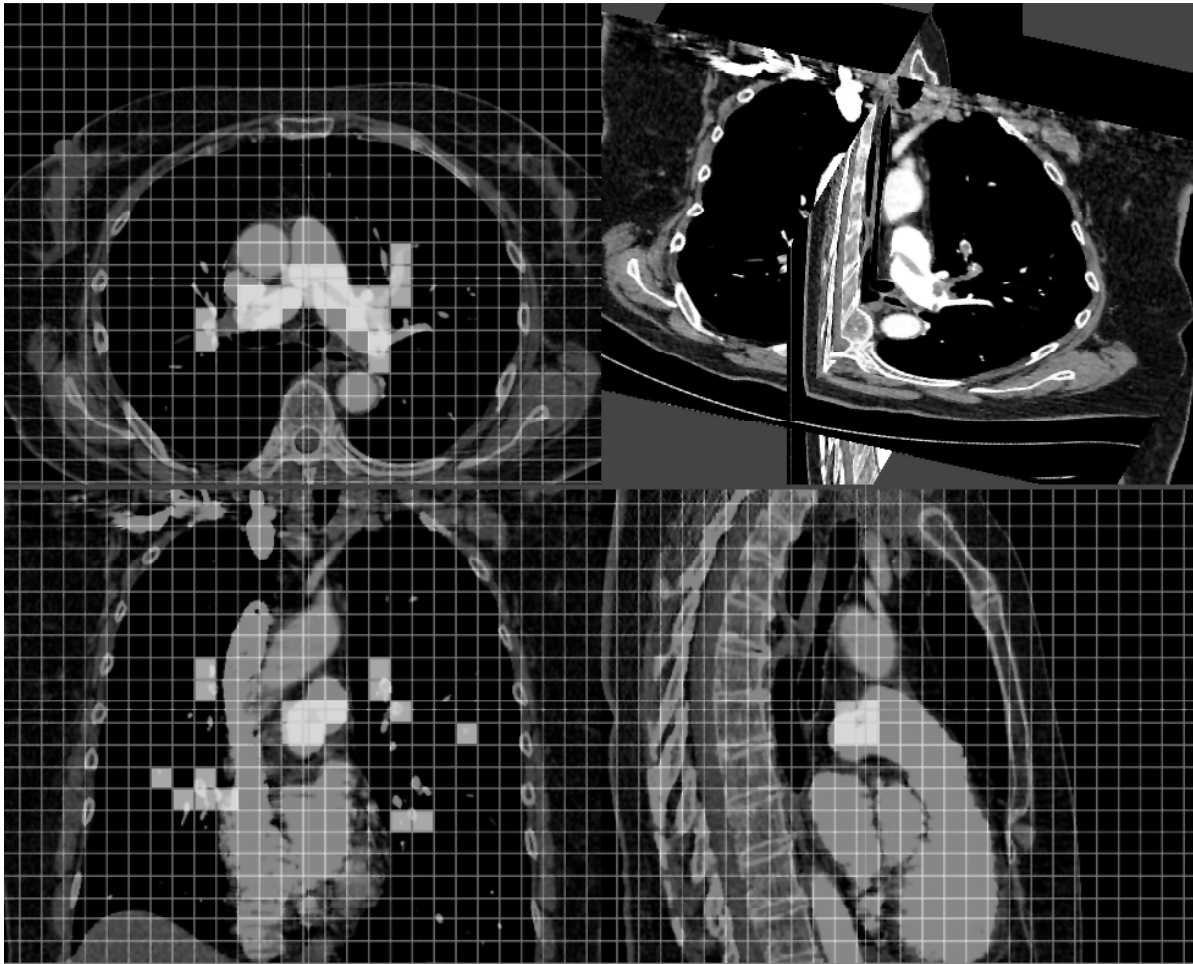


Figure 10: Creation of ground truth. A grid is super-imposed to the image date, the radiologist uses the mouse to highlight boxes of voxels whenever a clot (at least partially) belongs to it. Color is used in actual the application.

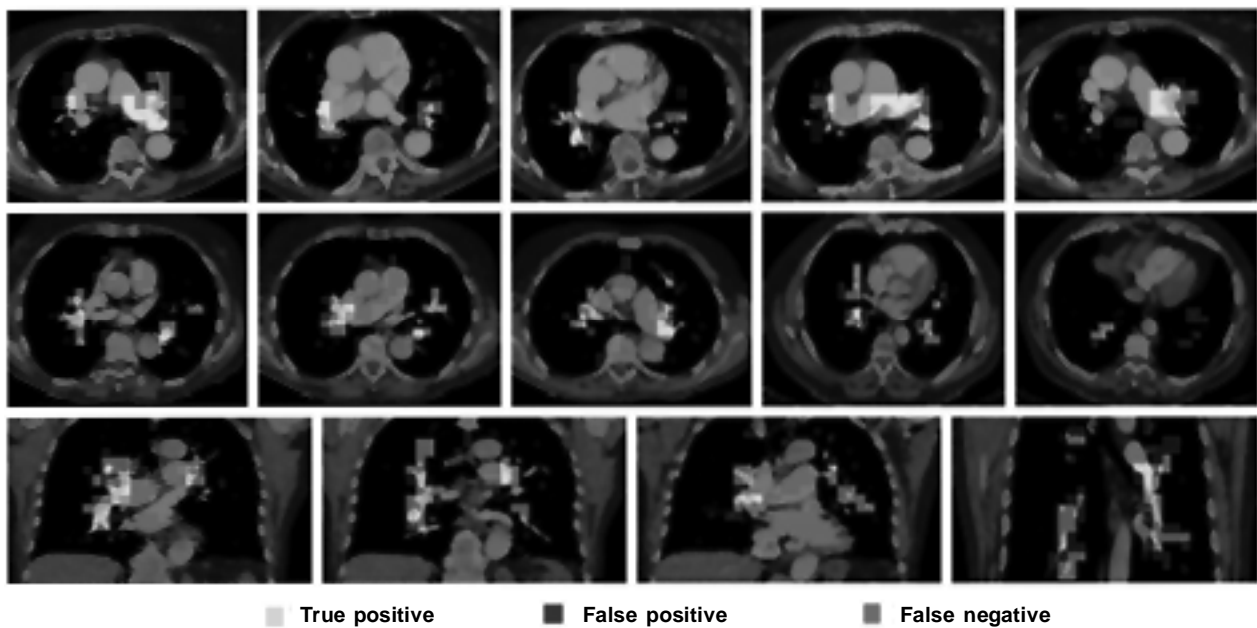


Figure 11: Analysis of detection results. Results are compared with ground truth data, false positives and negatives, and true positives are color mapped for easier interpretation. Non-detections (or false negatives) are painted in red, while false alarms are in blue.

positives, but misses more and more clots as ones goes farther in the PA. This is because the clot takes a bigger part of the section of the vessel when the size of the vessel decreases, and it does not create a concavity anymore. Moreover, the segmentation may stop early in vessels that are obstructed by clots, leaving *M1* useless for the remaining of the vessel. In contrast, method *M2* detects clots everywhere as long as their shape are compatible with its hypothesis. *M2* gives a lot of false positives and few non-detections. Yet, *M1* can detect clots that form concavities, that *M2* cannot when its shape criterion is not met, and this increases the overall sensitivity. Detection rates for each methods considered separately actually depend on where the clots reside in the PA, and their ranges are given for illustrative purpose: [0%, 51%] for *M1*, [57%, 100%] for *M2*.

Table 1
CPU Time for each Algorithm

<i>Method</i>	<i>Time</i>
PA Segmentation	35 seconds
M1 Detection	7 minutes
Lung Semgmentation	12 seconds
M2 Detection	6 minutes and 45 seconds

Yet, *M2* accounts for most of interesting detections for the radiologist. This is because clots in the main parts of the PA are generally obvious to the radiologist, while peripheral clots generally require higher attention to detect, and are generally out of reach for *M1*.

This overall method is of interest to the radiologist if it can find most clots above a certain detection threshold and at the same time if it does not provide too many false positives. This first figure can be improved by using other features than the ones used in *M1* or *M2*, that would provide a rough initial detection step, step that would be followed by a more advanced classification approach to decrease the false alarm rate.

5.2 Computational Expense

In terms of processing time, which depends on the size of the data, results are given in Table 1. The processor used for these tests is a PowerPC 970 running at 1.8 GHz, with 2 GB of RAM, and the algorithms were implemented in the C language.

The computational complexity of the method is proportional to the size of the data.

6. CONCLUSION

We have presented a framework for semi-automatic detection of pulmonary embolism. Two detection methods were implemented, the first one being based on an original model-based segmentation of the pulmonary arteries, the second using simple shape hypothesis. These methods were then combined to provide the final detection decision. An

evaluation scheme was proposed for the PE detection problem, which consists of a way to making ground truths, by a radiologist, on a lower resolution 3D grid and performance was assessed in terms of sensitivity and specificity.

This method provides valuable help to the radiologist, by highlighting clots candidates that he might have missed, enabling more accurate diagnosis of PE.

A possible extension to this work could be to make the method more conservative by relaxing the search criteria, then provide its output to the input of a classifier for emboli presence.

ACKNOWLEDGMENT

This work is supported by the R'egion Wallonne of Belgium and the European Social Funds.

NOTES

1. make them appear white in the image
2. This slice concept is not to be confused with slices of CT images.
3. this can be done with other curves as well by augmenting point multiplicity, but this is less intuitive
4. vessel part between two bifurcations

REFERENCES

- [1] E. Coche, "Evaluation of multislice CT for the diagnosis of pulmonary embolism," Ph.D. dissertation, Université catholique de Louvain, Faculté de Médecine, Apr. 2005.
- [2] J. A. Sethian, *Level Set Methods and Fast Marching Methods*. Cambridge University Press, 1999.
- [3] J. Serra, *Image Analysis and Mathematical Morphology*. Academic Press, 1982.
- [4] C. Kirbas and F. K. H. Quek, "A review of vessel extraction techniques and algorithms," VISLab, Wright State University, Dayton, Ohio, Tech. Rep., Nov. 22 2000. [Online]. Available: <http://vislab.cs.wright.edu/review/Extraction/extractionReview.pdf>
- [5] P. Felkel, "Segmentation of vessels in peripheral CTA datasets," VRVis Center, VRVis Technical report TR-VRVis-2000-008, Dec. 2000.
- [6] C. Zahlten, H. Juergens, and H. O. Peitgen, "Reconstruction of branching blood vessels from ct-data," *Proceedings of the Eurographics Workshop on Visualization in Scientific Computing, Rostock*, pp. 41–52, June 1994.
- [7] R. Malladi, J. Sethian, and B. Vemuri, "Shape modeling with front propagation: A level set approach," *IEEE Transactions on Pattern Analysis and Machine Intelligence*, vol. 17, no. 2, pp. 158–175, Feb. 1995.
- [8] T. Deschamps and L. Cohen, "Fast extraction of tubular and tree 3d surfaces with front propagation methods," in *16th International Conference on Pattern Recognition, ICPR'02*, Quebec, Canada, Aug. 2002.
- [9] T. Deschamps, L. Cohen, and S. Ebeid, "Fast surface segmentation of 3D tree structures with front propagation methods," in *Fifth International Conference on Curves and Surfaces*, Saint-Malo, France, June 2002.
- [10] R. Sebbe, B. Gosselin, E. Coche, and B. Macq, "Pulmonary arteries segmentation and feature extraction through slice marching," in *Proceedings of the 14th ProRISC workshop on*

- Circuits, Systems and Signal Processing (ProRISC 2003)*, Veldhoven (Netherland), Nov. 2003.
- [11] —, “Segmentation of opacified thorax vessels using model-driven active contour,” in *Proceedings of the 17th Annual International Conference of the IEEE Engineering in Medicine and Biology Society (EMBC 2005)*, Shanghai (China), Sept. 2005.
- [12] Y. Masutani, H. MacMahon, and K. Doi, “Computerized detection of pulmonary embolism in spiral ct angiography based on volumetric image analysis,” *IEEE Transactions on Medical Imaging*, vol. 21, no. 12, pp. 1517–1523, Dec. 2002.
- [13] J. Liang, M. Wolf, and M. Salganico”, “A fast toboggan-based method for automatic detection and segmentation of pulmonary embolism in ct angiography,” in *Int. Conf. on Medical Image Computing and Computer Assisted Intervention (MICCAI’05)*, Palm Springs, USA, Oct. 2005.
- [14] B. van Ginneken, A. Frangi, J. Staal, B. Haar, and R. Viergever, “Active shape model segmentation with optimal features,” 2002.
- [15] “Kdd cup task: Computer aided detection of pulmonary embolism,” Computer-Aided Diagnosis and Therapy Group-Siemens Medical Solutions, Malvern (PA). Available on: <http://www.cs.unm.edu/files/kdd-cup-2006-task-spec-v1.pdf>, 2006, may 15, 2006.
- [16] O. Cuisenaire, “Distance transformations: Fast algorithms and applications to medical image processing,” Ph.D. dissertation, Université catholique de Louvain, Faculté des Sciences, October 1999.
- [17] F. L. Bookstein, “Principal warps: Thin-plate splines and the decomposition of deformations,” *IEEE Transactions on Pattern Analysis and Machine Intelligence*, vol. 11, no. 6, pp. 567–585, 1989.
- [18] C. Tomasi and R. Manduchi, “Bilateral filtering for gray and color images,” in *Proceedings of the 1998 IEEE International Conference on Computer Vision, Bombay (India)*, 1998.
- [19] O. Cuisenaire, “Locally adaptable mathematical morphology using distance transformations.” *Pattern Recognition*, vol. 39, no. 3, pp. 405–416, 2006.
- [20] R. Sebbe, “Computer-aided diagnosis of pulmonary embolism in opacified ct images,” Ph.D. dissertation, Faculté Polytechnique de Mons & Université d’Orléans, November 2006.